RSC Advances

PAPER

View Article Online
View Journal | View Issue

Cite this: *RSC Adv.*, 2022, **12**, 33889

Novel polyaniline–polyethersulfone nanofiltration membranes: effect of *in situ* polymerization time on structure and desalination performance

Ayyaz Shahbaz Butt, [a] Asif Ali Qaiser, *[b] Nida Abid[b] and Umer Mahmood[b]

In this research, novel polyaniline-layered nanofiltration membranes were prepared by phase inversion of base polyethersulfone (PES) membranes and subsequent *in situ* solution-phase deposition of polyaniline as a thin surface layer. In these composite membranes, the impact of the polyaniline deposition time on steric hindrance and electrostatic interactions during permeation was elucidated. The chemical structure, thermal stability, and mechanical properties of the PES and PANI-PES membranes were investigated using Fourier-transform infrared spectroscopy (ATR-FTIR), thermogravimetric analysis (TGA), and dynamic mechanical analysis (DMA), respectively. The membranes' porosity and pore size decreased as PANI deposition time increased. As PANI deposition time increased, PANI layered nanofiltration membranes exhibited improved thermal stability but deteriorated mechanical characteristics due to free radical destruction from prolonged exposure to the oxidant. These PANI–PES membranes showed 43% rejection (NaCl) at 1.7 bar coupled with a flux of 11.59 L h^{-1} m^2 that is quite promising when comparing with similar Nanofilteration (NF) membranes in the literature and commercial NF membranes, as well. As the deposited layer, PANI is partially doped; hence, permeation results have been interpreted in terms of steric hindrance and electrostatic repulsion by electrochemical PANI layering.

Received 11th September 2022
Accepted 17th October 2022

DOI: 10.1039/d2ra05735b

rsc.li/rsc-advances

1. Introduction

Water is a valuable resource for human life that is becoming increasingly scarce day by day. It is also crucial for the survival of all species on earth, as well as for economic, social progress, and environmental sustainability.[1] Rapid industrialization, agricultural activities, natural salt deposits, and population growth are major causes of water shortage and the driving force for the advancement of technologies for exploiting alternate water resources, such as desalination of saline water.[2–4] Desalination is also used to improve the quality of freshwater. Thermal and membrane-based technologies such as flash evaporation, reverse osmosis, electrodialysis, and nanofiltration are the most common methods used for desalination of water.[5,6]

Nanofiltration (NF) has emerged as one of the most promising membrane technologies owing to its multiple advantages such as low operating pressure, high permeation flux, high retention of multivalent ions and organic molecules with molecular weight between 100 and 1000 Da. In addition, low capital investment and operational/maintenance expenses have made NF an attractive purification process for industry. As a result of these advantages, the usage of NF has grown around the world and now accounts for 10% of the global brackish water market.[7–9] The augmentation of nanofiltration membranes into other desalination methods such as reverse osmosis, forward osmosis, electrodialysis, multi-stage distillation, multiple-effect desalination, membrane distillation, and ion exchange improves the quality of freshwater and reduces both operating pressure and membrane fouling. There have been significant efforts put into the synthesis of low-pressure, low-cost, and easy-to-prepare NF membranes.[10–12]

Nanofiltration membranes are categorized into two major groups that are (1) integrally skinned asymmetric membranes and (2) thin-film composite (TFC) membranes. TFC membranes are prepared by layer-by-layer deposition, interfacial polymerization (IP), *in situ* oxidative or electrochemical polymerization, electron beam irradiation, spin coating, dip-coating, plasma-induced polymerization, and UV-induced graft polymerization methods.[13,14]

Commercial nanofiltration (NF) membranes comprise of a thin film composite (TFC) structure with an ultra-thin polyamide layer on a microporous polysulfone substrate. The structural and physicochemical features of this ultra-thin polyamide film are directly associated with the separation performance of TFC-NF membranes in terms of permeability and selectivity. Interfacial polymerization (IP) is used to create a selective polyamide layer at the interface through the reaction of two insoluble monomers.[15,16] In contrast, the efficiency of this method is lower because of a non-uniform pattern of charge

[a]*Department of Chemical Engineering, University of Engineering and Technology, Pakistan*

[b]*Department of Polymer and Process Engineering, University of Engineering and Technology, 54890 Lahore, Pakistan. E-mail: asifaliqaiser@uet.edu.pk*

and polymer density of this selective layer. Furthermore, the interfacial polymerization process increases surface roughness of the membrane thus making the surface more prone to fouling.[17]

Composite membranes comprising of intrinsically conducting polymers (ICPs) such as polyaniline have also been used in a variety of applications such as electrodialysis, solvent separation, and acid-base separation.[18–20] Polyaniline (PANI) is one of the most widely used ICPs in membranes and has high electrical conductivity, electrochemical activity, excellent environmental and solution stability, low synthesis cost, and the ability to electrochemically switch between conductive and non-conductive states through a doping/dedoping process.[21–24]

Nanofiltration and ultrafiltration (UF) membranes for water treatment have been synthesized using polyvinylidene fluoride (PVDF), polyvinyl alcohol (PVA), polyacrylonitrile (PAN), polypropylene (PP), polysulfone (PSF), and polyethersulfone (PES). PES membranes have been widely employed because of their high mechanical strength, good chemical resistance, high thermal stability, environmental tolerance, and ease of fabrication.[25,26] The smaller size of the salt ions relative to the surface pore size of the membranes makes PES-based UF membranes unsuitable for desalination. PES-based UF support membrane can be used for desalination by depositing a thin hydrophilic polymer layer on this base.[27,28] On the other hand, PES blends with various nanoparticles (ZnO, TiO_2, GO, Fe_3O_2, ZrO_2, and Al_2O_3, *etc.*) have shown significant improvement in water permeability and salt rejection.[29–31]

Polyaniline (PANI) based composite membranes have been fabricated and trialed for various applications including desalination, solvent separation, electrodialysis, wastewater treatment *etc.*[32–35] Zhi Wang *et al.*, prepared PANI/polysulfone (PSU) nanocomposite membranes to study their effectiveness for desalination. These nanocomposite membranes were prepared through the filtration of PANI nanofiber aqueous dispersion with PSU substrate membrane. In these membranes, PANI nanofibers are assembled evenly on the PS membrane surface and porous structures were formed.[36] Performance of polysulfone membranes was improved by blending with PANI nanofibers in wt% ranging 1–15%. PANI nanofibers assembled as finger like structure in these PANI–PS membranes. The blended membranes had higher porosity and pore size as compared to base PSU membranes.[37] Permeation flux and salt rejection of polysulfone based ultrafiltration membranes were improved with nanostructured polyaniline. These composite membranes were prepared by blending PANI nanoparticles in PSU dope solution. The negatively charged PANI increased porosity, and hydrophilicity that improved permeability and surface charge on membrane resulted in improved salt rejection.[38] Adsorptive behavior of polyaniline has been utilized to capture various heavy metals and ions such as chromium, arsenic, mercury and various radioactive metal ions in wastewater treatment to meet the safe water quality standards.[39] These membranes were synthesized by blending polyaniline particles, with a polymer for solution casting of the membranes.[40] These membranes had a dense morphology with smaller and fewer pores and the incorporation of PANI led to a progressive expansion of pores and an increase in porosity. The effects of *in situ* polymerization of aniline and its conditions on the deposition extent of PANI on various base membranes and their electrochemical and electrodialytic performance have been discussed using various substrates including poly(vinylchloride-*co*-vinylacetate), polyvinylchloride, thermoplastic polyurethane, and cellulose acetate.[41–45]

The present research employed *in situ* polymerization to deposit polyaniline as a thin film on base polyethersulfone nanofiltration membranes. The synthesis of PANI layered membrane using PES nanofiltration substrate through *in situ* oxidative polymerization has been reported first time in literature for nanofiltration desalination applications. PANI–PES membranes were synthesized using a three-step methodology to facilitate PANI layering at the substrate membrane; (1) fabrication of polyethersulfone asymmetric nanofiltration membrane by phase inversion method (2) surface activation of asymmetric nanofiltration membranes using sodium hydroxide and (3) conversion of hydrolyzed asymmetric nanofiltration membrane into PANI layered nanofiltration membrane by depositing polyaniline through *in situ* solution-phase polymerization. The synthesis was followed by mechanical, chemical, thermal, and morphological characterizations, and testing membranes performance in a dead-end stirred cell for desalination. The results showed a significant effect of PANI deposition and polymerization time on the composite membranes structure, mechanical properties, and desalination performance.

2. Experimental

2.1. Materials

Polyethersulfone (PES, Ultrason® E7020P, molecular weight = 92 000 g mol^{-1}) was kindly provided by BASF Pakistan. *N*-Methyl-2-pyrrolidone (NMP) acquired from VWR (Belgium) was used as a solvent to prepare PES dope solution. Sodium hydroxide (NaOH) was purchased from DaeJung (Korea) and sodium chloride (NaCl) was acquired from Merck (USA). Hydrochloric acid (37% conc.) and aniline were purchased from Sigma Aldrich (USA) and used as received. Ammonium persulfate (APS) was obtained from Merck (USA). The nonwoven backing layer (thickness = 180 μm, Novae 2471) of polypropylene/polyethylene (PP/PE) was acquired from Freudenberg (Germany). For all experiments, RO treated water of <5 ppm TDS was used.

2.2. Fabrication of polyethersulfone nanofiltration membranes

PES membranes were synthesized using phase inversion technique. Polyethersulfone (PES) was dried at 150 °C for 4 hours in a vacuum oven and PES dope solution was prepared by dissolving 24% (w/w) PES in NMP using a hot plate with continuous stirring at 40 °C for 15 hours. The solution was then degassed for 48 hours to ensure to remove entrapped air. The degassed dope solution was poured on non-woven fabric support made of PE/PP (thickness = 180 μm, Novae 2471) and

cast at 37 °C with 35% relative humidity using Sheen® film applicator. The solvent from the wet membrane was partly evaporated in the open air for 1.5 minutes. The membranes were then placed in a water bath for 24 hours to separate the phases. The water in the coagulation bath was continuously replenished to guarantee that the NMP was entirely removed.[32,33]

2.3. Surface activation of PES membranes

A solution of 2 M NaOH was used as a surface activator to provide hydrophilicity to polyethersulfone membranes. The membranes were soaked in NaOH solution at 37 °C for 17 hours, and then washed with an excess of RO treated water to remove any extra NaOH on the surface.[34,46–48]

2.4. Deposition of polyaniline on surface activated PES membranes

To prepare PANI layered nanofiltration membranes, *in situ* polymerization of aniline was carried out on the surface of surface-active hydrolyzed PES membranes (HPES). A thin layer of PANI was deposited on the surface of HPES by soaking it in a 4% v/v solution of aniline in 1 M HCl for 24 hours at 25 °C. After that, a 0.55 M APS solution (in 1 M HCl) was added to aniline solution at 25 °C for varying polymerization time (30–150 mins). The free monomers were rinsed with a solution of 1 M HCl, and the membranes were washed three times with water.[22,38] The steps involved in PANI–PES membranes fabrication are shown in Fig. 1.

In the following text, PANI–PES membranes are designated using PANI-XXM-P nomenclature where PANI shows polyaniline coating on PES substrate, XXM specifies polymerization time of aniline in minutes after APS addition, and P indicates *in situ* polymerization reaction, respectively.

2.5. Membranes characterization

Membranes porosity was measured using dry–wet (gravimetric) method. The membranes were weighed after drying and wetting with water using an electronic balance (model: HL-323A+).

The porosity of the membranes (ε) was calculated using the following equation:[49,50]

$$\varepsilon = \frac{W_{\text{wet}} - W_{\text{dry}}}{V_{\text{membrane}} \times \rho_{\text{water}}} \quad (1)$$

where W_{dry} and W_{wet} are the weights of dry and wet membranes in kg, V_{membrane} is volume of the membrane (m^3) and ρ_{water} is the density of water (kg m^{-3}) at room temperature.

The average pore size, R_M has been estimated using filtration velocity method that involves measuring pure water flux (PWF) of membrane by applying pressure (15 bar) for a specified time. Based on pure water flux (eqn (3)) and porosity data, the Guerout–Elford–Ferry equation (eqn (2)) was used to calculate membrane mean pore radius (R_M, m):[32,51]

$$R_M = \sqrt{\frac{(2.9 - 1.75\ \varepsilon) \times 8\mu Q l_M}{\Delta P \varepsilon A_M}} \quad (2)$$

where μ, Q, P, ε, A_M and l_M denote water viscosity (Pa s), volumetric flow rate of permeate (m^3 s^{-1}), operating pressure (Pa), membrane porosity, membrane effective area and membrane thickness, respectively.

Membranes surface chemistry was studied by Fourier transform infrared spectroscopy (FTIR) using JASCO FT/IR-4600 spectrometer in attenuated-total-reflectance (ATR) mode with zinc selenium (ZnSe) crystal as the background operating in 400–4000 cm^{-1} wavenumber range.

Thermal stability of PANI–PES membranes was characterized using SHIMADZU TGA-50 Thermogravimetric Analyzer. A 5 mg sample was placed on an aluminium (Al) pan and heated to

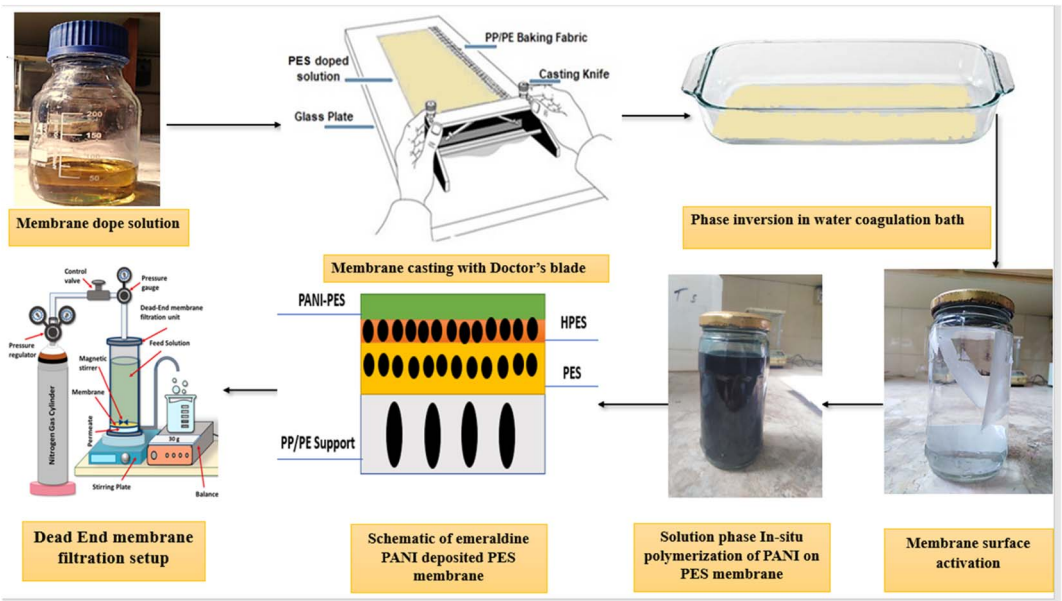

Fig. 1 Schematics of PANI–PES membranes fabrication and performance evaluation.

600 °C at a rate of 10 °C min^{-1} in a nitrogen environment (35 mL min^{-1}).[52,53]

Mechanical properties of the membranes were evaluated using TA Q800 DMA (dynamic mechanical analyzer) operated in tensile (UTM) mode using 10 mm × 50 mm samples. The test temperature was kept at 37 °C with a constant strain rate of 100 mm min^{-1} and tensile strength, elastic modulus, and elongation-at-breakpoint (%) were measured.

2.6. Nanofiltration performance of PES and PANI–PES membranes

Desalination performance of the membranes was evaluated using a dead-end filtration cell. This laboratory setup comprised of a gas cylinder, pressure control valve, membrane cell, magnetic stirrer, and a feed spacer (Fig. 1). The cell was filled with feed water and pressurized with nitrogen gas. The permeate stream was collected into a permeate cylinder. Before each experiment, the membranes were soaked in treated water for 2 hours to provide saturation and wettability. Each membrane was initially pre-compacted in treated water for 30 min at 12 bar. Pure water permeability (PWP) was determined at 15 bar and the following equations were used to calculate PWP, solvent flux (J_S), and salt rejection (SR) respectively:

$$\mathrm{PWP} = \frac{V_{\mathrm{permeate}}}{A_M \Delta t \Delta P} \quad (3)$$

$$J_{\mathrm{solvent}} = \frac{V_{\mathrm{permeate}}}{A_M \Delta t} \quad (4)$$

$$\mathrm{SR}\ (\%) = \left(1 - \frac{C_P}{C_F}\right) \times 100 \quad (5)$$

where C_P, C_F and are the concentrations of permeate and feed in ppm whereas V_{permeate} (liter) is the volume of permeate collected in time Δt (h).

3. Results and discussion

3.1. Porosity and pore size

The values of porosity of PES–PANI membranes are given in Table 1. The porosity decreased from 73.41% for pristine PES membrane to 55.86% for PANI–PES membranes (Table 1). Pristine PES membrane had an average pore size of 5.90 nm that reduced to 4.24 nm on polyaniline deposition. The porosity and pore size of the membranes reduced as PANI deposition time increased that increased PANI layering extent on HPES membrane, attributed to a strong attraction between –NH groups of polyanilines and –OH groups of HPES.[54,55]

Table 1 Porosity and mean pore size of membranes

Membrane samples	Porosity (%)	Mean pore size (nm)
Pristine PES	73.41	5.90
PANI-30M-P	64.05	4.78
PANI-60M-P	62.88	4.52
PANI-90M-P	61.42	4.72
PANI-120M-P	59.96	4.45
PANI-150M-P	55.86	4.24

3.2. FTIR-ATR spectroscopy

Fig. 2 shows FTIR spectra of PES, HPES, and PANI–PES membranes. The IR band at 3637 cm^{-1} is attributed to O–H stretching of water molecules.[56–58] IR peaks relating to aromatic rings can be assigned to 839–1011 cm^{-1} (C–H bending in para-substituted aromatic ring), 1484 and 1577 cm^{-1} (C=C stretching), and around 3091 cm^{-1} (C–H stretching). The sulfone group (O=S=O stretching) shows characteristic peaks at 1149, 1238, and 1300 cm^{-1}, whereas aromatic ether shows peaks at 1103 cm^{-1} (C–O–C stretching) and at 705 cm^{-1} for C–S stretching.[59]

The peak shift from 3637 to 3433 cm^{-1} HPES membrane indicated hydrophilic character of polyethersulfone membrane when treated with sodium hydroxide due to the presence of hydrogen-bonded O–H stretching.[47,60]

The successful deposition of PANI on HPES membranes is indicated by quinonoid at 1564 cm^{-1}, benzenoid at 1471 cm^{-1} and polaron moieties at 1137 cm^{-1} respectively. The aromatic amine nitrogen (C–N stretching vibration) was indicated by peaks at 1240 and 1300 cm^{-1}.[61,62] As PANI deposition time on PES base membranes increased, the distinctive peaks of PANI became more pronounced.

3.3. Thermogravimetric analysis (TGA)

Fig. 3 shows TGA thermograms of pristine PES, HPES, and PANI–PES membranes.

Pristine PES membrane exhibited three weight loss regions at 65–75 °C, 185–250 °C, and 553–588 °C, respectively. The first weight loss may be attributed to entrapped water from the coagulation bath. The second weight loss could be attributed to entrapped solvent (*i.e.* NMP) and the third weight loss

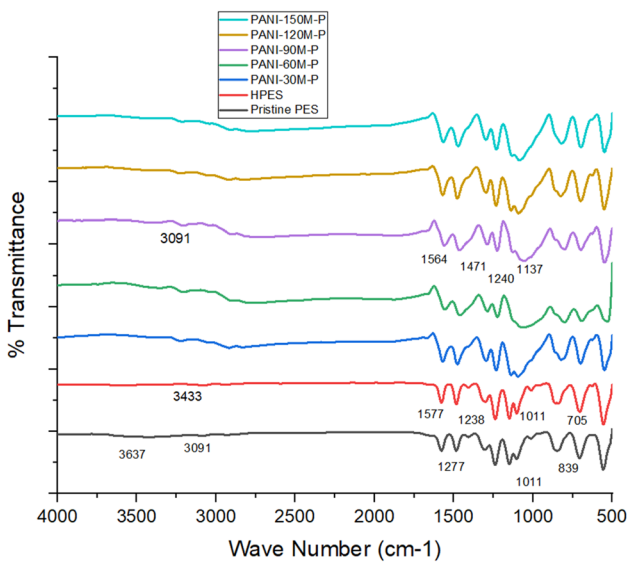

Fig. 2 FTIR-ATR spectra of unmodified PES, HPES, and PANI–PES membranes.

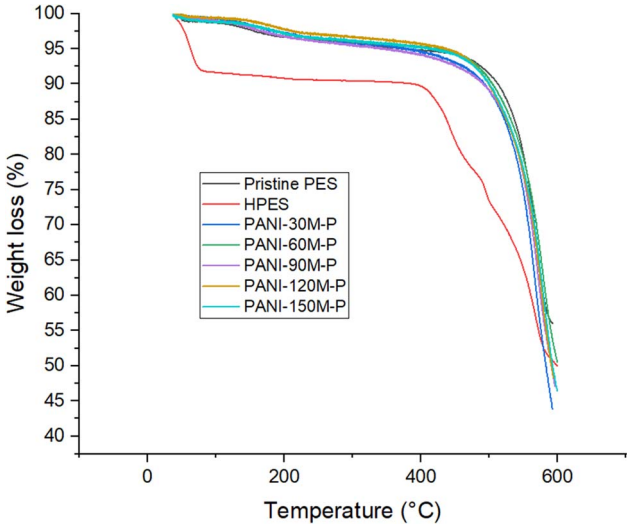

Fig. 3 TGA analysis of pristine PES, HPES and PANI coated PES membranes.

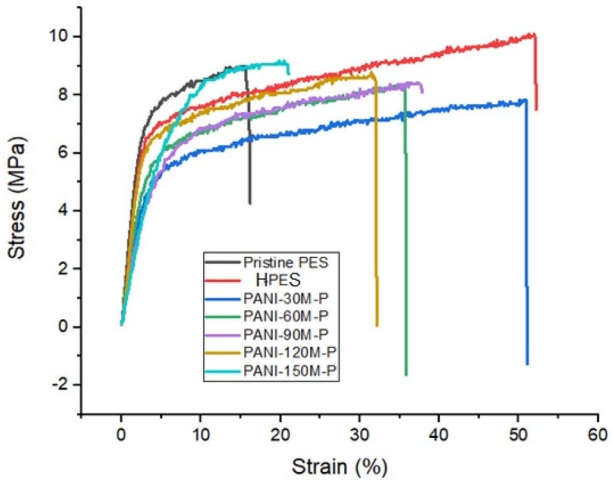

Fig. 4 Stress–strain curves of unmodified PES and PANI–PES membranes.

confirmed the decomposition of PES backbone structure.[52,63] The TGA curve of surface-activated PES also showed three-step thermal degradation. The first step shown between 43 and 100 °C (water evaporation), the second at 400 to 500 °C that is attributed to the decomposition temperature of the self-associated hydroxyl group (–OH),[64] and the temperature at 500 to 580 °C is decomposition temperature of polyethersulfone backbone.

For polyaniline-coated PES membranes, a three-step thermal degradation mechanism was shown. The initial weight loss at 125–275 °C is attributed to loss of water residing in the membrane structure and loss of dopant anions whereas, the second degradation step from 360–490 °C can be attributed to the degradation of the PANI main chains.[65,66] The third step at >500 °C indicated degradation of main PES molecular chains.

Increasing PANI deposition time shifted TGA curves towards a slightly higher degradation temperature of polyethersulfone. Moreover, the decomposition behavior of polyethersulfone in pristine PES and PANI–PES membranes remained identical.

3.4. Mechanical characterization of the membranes

The stress–strain curves of pristine PES, HPES, and PAN–PES are shown in Fig. 4 where Table 2 shows values of tensile strength (σ_T), Young's modulus (E_M), and elongation at break (ε_B) calculated from these curves. Young's modulus was determined from the initial slope within Hooks law limit of the stress–strain curve.

Sodium hydroxide-modified PES membranes showed significantly higher elongation probably because of a self-associated hydroxyl group (–OH) that increased film's mechanical properties.[47]

Prolonging PANI deposition time on PES membranes reduced elongation to break values and tensile strength as well. This decrease can be attributed to the brittle character of PANI along with possible molecular chain scission of base PES by free-radical attack generated from the decomposition ammonium persulfate that was used as oxidant in polymerization reaction.[67]

Table 2 Mechanical properties of PES and PANI–PES membranes

Membrane identity	Tensile strength (MPa)	Elastic modulus (GPa)	Elongation at break (ε_B) (%)
Pristine PES	9.00	3.46	16.20
HPES	10.00	2.46	52.21
PANI-30M-P	7.84	1.67	51.00
PANI-60M-P	8.32	2.75	35.86
PANI-90M-P	8.42	2.75	37.86
PANI-120M-P	8.77	3.25	32.13
PANI-150M-P	9.17	3.46	21.00

3.5. Separation performance of PANI–PES NF membranes

The salt rejection study of PANI–PES membranes using a feed (1900 ppm NaCl) was carried out using a dead-end stirred cell at 17 bar.[68,69] This feed concentration represents low-salinity fresh and brackish water feeds. Table 3 shows flux and % salt rejection from PES and PANI–PES membranes. Pristine PES membrane showed 36.84% salt rejection, whereas PANI–PES membranes showed 43.42% rejection. This increase in membrane salt rejection is because of the deposition of a thin

Table 3 Salt rejection and flux of PES and PANI–PES membranes

Membrane samples	Water flux (L h^{-1} m^{-2})	% NaCl rejection
Pristine PES	25.73	36.84
PANI-30M-P	20.45	38.68
PANI-60M-P	17.46	39.47
PANI-90M-P	16.19	40.84
PANI-120M-P	14.11	41.84
PANI-150M-P	11.59	43.42

polyaniline layer on PES membrane surface through *in situ* oxidative aniline polymerization that reduced membrane porosity and average pore diameter (Table 1). During *in situ* polymerization, PANI particles grew in size forming a globular structure following a well-defined nucleation and growth mechanisms.[70] This growth of PANI first created a very thin layer, which developed in thickness due to the second nucleation as a result of the prolonged polymerization period. It is assumed that PANI layering at the surface of PES membranes offered a significant resistance to salt solution permeation by blocking pores and reducing porosity.[19] The increase in salt rejection can also be attributed to the adsorptive behavior of polyaniline and its negatively charged surface.[71] The adsorptive behavior tends to capture salt ions on the membrane surface forming a thin salt layer that offers further hindrance to permeating salt and water molecules thus increasing the salt rejection but at the expense of reducing water flux. The Na^+ ions has also been captured by negative charges of PANI surface layer. Moreover, the increase in negative charge on membrane surface due to the presence of anion-doped polyaniline repelled negatively charged Cl^- in feed.[72] Polyethersulfone membranes have a negative surface charge and their separation mechanism is influenced not only by steric hindrance but also by electrostatic interactions (*i.e.*, Donnan exclusion).[32] The existence of strong electrostatic repulsive force between the negatively charged membranes and divalent anions led to a relatively high rejection of hydrated divalent anions.[73] Therefore, smaller pore size increases the rejection of salts through both size exclusion and electrostatic repulsion mechanisms.[32,58] An overall 18% increase in salt rejection was achieved that is a cumulative effect of size exclusion or Donnan effect due to porosity and pore size reduction and charge exclusion imparted by permanent membrane negative charge.[74] The significant decrease in flux is in line with the surface coverage of the base membrane with PANI that increases with an increase in polyaniline deposition time. As permeability of the nanofiltration membranes follows both pore flow and solution diffusion models, the flux of PANI–PES membranes can be explained by both models separately.[75,76] In case of pore flow mechanism, higher the porosity and larger the pore size, less resistance is offered to permeating molecules. The rate of flux decrease is directly linked to the surface layer deposition extent and density. Denser and thicker PANI layer on prolonging polymerization time exponentially reduces membrane flux as can be seen in Table 3.[77,78] On the other hand, explaining salt and water permeation through nanofiltration membranes using solution–diffusion mechanism necessitates that the surface of nanofiltration membranes should be hydrophilic in nature that can facilitate water

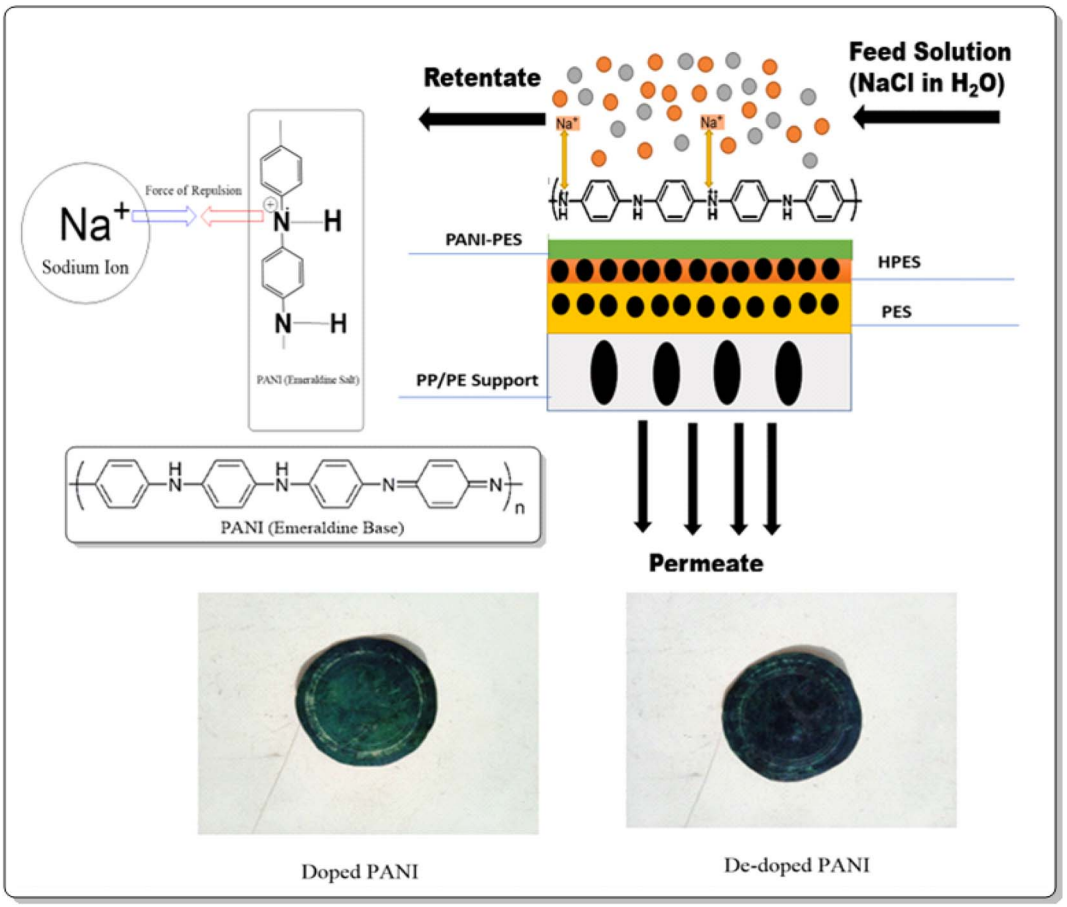

Fig. 5 PANI–PES interaction and electrostatic effects of pristine PES and PANI–PES membranes.

Table 4 Comparison of present PANI–PES membranes performance with nanofiltration membranes in literature

Membrane type	Flux (L m^{-2} h^{-1})	% NaCl rejection	Permeation conditions	Ref.
Pristine PES membrane	**25.73**	**36.84**	***P* = 1.7 MPa Feed = 1900 ppm**	**Present study**
PANI–PES membrane	**11.59**	**43.42**	***P* = 1.7 MPa Feed = 1900 ppm**	**Present study**
PES NF membranes	54.88	22.0	$P = 2.0$ MPa Feed = 10 500 ppm	32
Nanotube/polyethersulfone nanocomposite oxidized multiwalled carbon (asymmetric NF membrane)	8.0	20.0	$P = 0.4$ MPa Feed = 200 ppm	81
Multiwalled nanotubes with amine-functionality (asymmetric NF membrane)	5.241	20.0	$P = 0.4$ MPa Feed = 200 ppm	82
NF90 (Filmtech, Dow, TFC)	80.0	22.0	$P = 1$ MPa Feed = 800 ppm	83
DS-5 DL (nanofiltration TFC)	19.2	1.31	$P = 1.4$ MPa Feed: seawater	84
NE2540-70 (nanofiltration TFC)	18.0	7.20	$P = 1.4$ MPa Feed: seawater	84
PES–PA–PANI blended TFC NF	55.2	28.5	$P = 0.6$ MPa Feed: 2000 ppm	87

molecules to be (1) absorbed on the surface, (2) diffused through the thickness on the basis of chemical potential difference on either sides and (3) desorbed on the downstream side. PES is intrinsically hydrophobic in nature therefore the modification with NaOH imparts some hydrophilicity. This generated hydrophilic part of PES membranes has been utilized by polyaniline molecules during deposition mechanism where PANI grew on the surface by bonding with the hydrophilic surface functionality. Similarly PANI is intrinsically hydrophilic in nature in its doped form and surface hydrophilic content depends on dopant nature and dopant loading.[79] In PES–PANI membranes, PANI was doped with HCl that makes it partial hydrophilic[80] thus helps in water molecules absorption and diffusion during permeation at slower rate. Because of HCl leaching, PANI becomes dedoped and loses its hydrophilicity as well as the surface charge character[15] becoming less effective for water molecules permeability and loss of surface charge also reduces the salt rejection as compared to doped PANI (Fig. 5). Moreover, during PANI deposition, the PES membrane surface and pores are initially wetted with anilinium solution that subsequently reacts with oxidant therefore pore blockage is possible along with predominant surface deposition. The loss in membrane permeability is a combined effect of surface deposition, pore blockage, and hydrophilicity loss owing to HCl leaching (Fig. 5).

PANI layering on PES support led to a positive charge accumulation thus repels co-ions (cations) and to preserve charge neutrality, a few negatively charged ions remained in the solution. This electrostatic mechanism allows membranes to reverse the effect of increased pore size, porosity, the hydrophilicity of membranes which increases water permeability.[59,60]

Table 4 shows a comparison among different NF membrane systems with that of the present PANI–PES membranes in terms of permeation flux and NaCl rejection at various feed conditions. This comparison shows that the NF membranes desalination performance is a function of membrane morphology and functional fillers added to the base membrane matrix thus indicating the validity of both pore-flow and solution–diffusion models discussed above. The similar comparisons are given in literature[85] where the effect of feed concentration showed negligible effect on membrane rejection performance.[85,86] In addition, the flux and rejection values of pristine PES indicate the asymmetric membranes structure with decreasing pore size at the surface thus blocking the passage of salt ions. Layering of PANI through *in situ* deposition enhanced these blocking effects as discussed above and shown in Table 3 as a function of aniline polymerization time.

4. Conclusion

In situ aniline polymerization was used to deposit electroactive polyaniline (PANI) over polyethersulfone (PES) base membranes to create PANI layered membranes. The effects of polymerization time on PANI layering and performance of the membranes were elaborated. The base PES membranes were prepared by phase inversion coagulating in a non-solvent bath. The PANI-layered membranes showed improved thermal stability as measured by TGA. However, the mechanical properties decreased by increasing PANI deposition time because of macromolecular chains scission by free radical generated in the polymerization reaction. The FTIR-ATR spectra indicated increased PANI layering by prolonging aniline polymerization time with PANI deposited as conductive emeraldine salt. The porosity and pore size, both, decreased by increasing PANI deposition time. PES–PANI membranes showed the highest rejection of NaCl at 150 minutes of aniline polymerization time. However, the effect of PANI deposition was more pronounced on permeation flux as compared to the salt rejection. A comparison with other NF membranes indicated promising membranes performance by PANI layering on base PES NF membranes.

Conflicts of interest

There are no conflicts of interest to declare.

Acknowledgements

This work was funded as a fundamental research project through a grant provided by Higher Education Commission (HEC), Pakistan, under NRPU-HEC program.

References

1 F. Fu and Q. Wang, Removal of heavy metal ions from wastewaters: a review, *J. Environ. Manage.*, 2011, **92**(3), 407–418.
2 M. T. Amin, A. A. Alazba and U. Manzoor, A Review of Removal of Pollutants from Water/Wastewater Using Different Types of Nanomaterials, *Adv. Mater. Sci. Eng.*, 2014, **2014**, 825–910.
3 A. Ali, *et al.*, Membrane technology in renewable-energy-driven desalination, *Renewable Sustainable Energy Rev.*, 2018, **81**, 1–21.
4 D. Qadir, H. Mukhtar and L. K. Keong, Mixed Matrix Membranes for Water Purification Applications, *Sep. Purif. Rev.*, 2017, **46**(1), 62–80.
5 S. S. Shenvi, A. M. Isloor and A. F. Ismail, A review on RO membrane technology: developments and challenges, *Desalination*, 2015, **368**, 10–26.
6 P. Moradihamedani, *et al.*, High efficient removal of lead(II) and nickel(II) from aqueous solution by novel polysulfone/Fe_3O_4–talc nanocomposite mixed matrix membrane, *Desalin. Water Treat.*, 2016, **57**(59), 28900–28909.
7 P. M. Xuan, *et al.*, Effect of preparation conditions on arsenic rejection performance of polyamide-based thin film composite membranes, *Vietnam J. Sci. Technol.*, 2020, **62**(1), 7.
8 Y. He, *et al.*, Novel thin-film composite nanofiltration membranes consisting of a zwitterionic co-polymer for selenium and arsenic removal, *J. Membr. Sci.*, 2018, **555**, 299–306.
9 Y. He, *et al.*, UiO-66 incorporated thin-film nanocomposite membranes for efficient selenium and arsenic removal, *J. Membr. Sci.*, 2017, **541**, 262–270.
10 A. N. A. Mabrouk and H. E.-b. S. Fath, Techno-economic analysis of hybrid high performance MSF desalination plant with NF membrane, *Desalin. Water Treat.*, 2013, **51**(4–6), 844–856.
11 S. Sarkar and A. SenGupta, A new hybrid ion exchange–nanofiltration (HIX–NF) separation process for energy efficient desalination: process concept and laboratory evaluation, *J. Membr. Sci.*, 2008, **324**, 76–84.
12 S. Jabbarvand Behrouz, *et al.*, Carboxymethyl cellulose/polyethersulfone thin-film composite membranes for low-pressure desalination, *Sep. Purif. Technol.*, 2021, **269**, 118720.
13 A. W. Mohammad, *et al.*, Nanofiltration membranes review: recent advances and future prospects, *Desalination*, 2015, **356**, 226–254.
14 M. R. Esfahani, *et al.*, Nanocomposite membranes for water separation and purification: fabrication, modification, and applications, *Sep. Purif. Technol.*, 2019, **213**, 465–499.
15 F. Liu, *et al.*, A review: the effect of the microporous support during interfacial polymerization on the morphology and performances of a thin film composite membrane for liquid purification, *RSC Adv.*, 2019, **9**(61), 35417–35428.
16 H. Saitúa, *et al.*, Effect of operating conditions in removal of arsenic from water by nanofiltration membrane, *Desalination*, 2005, **172**, 173–180.
17 W.-P. Zhu, *et al.*, Poly(amidoamine) dendrimer (PAMAM) grafted on thin film composite (TFC) nanofiltration (NF) hollow fiber membranes for heavy metal removal, *J. Membr. Sci.*, 2015, **487**, 117–126.
18 D. Pile and A. Hillier, Electrochemically modulated transport through a conducting polymer membrane, *J. Membr. Sci.*, 2002, **208**, 119–131.
19 P. He, *et al.*, *In situ* growth of double-layered polyaniline composite membrane for organic solvent nanofiltration, *Chem. Eng. J.*, 2021, **420**, 129338.
20 E. Gungormus and S. Alsoy Altinkaya, A high-performance acid-resistant polyaniline based ultrafiltration membrane: application in the production of aluminium sulfate powder from alumina sol, *Chem. Eng. J.*, 2020, **389**, 124393.
21 M. Sairam, *et al.*, Polyaniline Membranes for Separation and Purification of Gases, Liquids, and Electrolyte Solutions, *Sep. Purif. Rev.*, 2006, **35**(4), 249–283.
22 M. A. Shehzad, *et al.*, *In situ* solution-phase polymerization and chemical vapor deposition of polyaniline on microporous cellulose ester membranes: AFM and electrical conductivity studies, *Synth. Met.*, 2015, **200**, 164–171.
23 M. S. Malik, A. A. Qaiser and M. A. Arif, Structural and electrochemical studies of heterogeneous ion exchange membranes based on polyaniline-coated cation exchange resin particles, *RSC Adv.*, 2016, **6**(116), 115046–115054.
24 D. K. Bandgar, *et al.*, Facile and novel route for preparation of nanostructured polyaniline (PANi) thin films, *Appl. Nanosci.*, 2014, **4**(1), 27–36.
25 Y. Orooji, *et al.*, Nanostructured mesoporous carbon polyethersulfone composite ultrafiltration membrane with significantly low protein adsorption and bacterial adhesion, *Carbon*, 2017, **111**, 689–704.
26 S. R. Mousavi, M. Asghari and N. M. Mahmoodi, Chitosan-wrapped multiwalled carbon nanotube as filler within PEBA thin film nanocomposite (TFN) membrane to improve dye removal, *Carbohydr. Polym.*, 2020, **237**, 116128.
27 H. Wang, *et al.*, Surface chemistry, topology and desalination performance controlled positively charged NF membrane prepared by polydopamine-assisted graft of starburst PAMAM dendrimers, *RSC Adv.*, 2016, **6**(6), 4673–4682.
28 T. Li, *et al.*, *In situ* coating TiO_2 surface by plant-inspired tannic acid for fabrication of thin film nanocomposite nanofiltration membranes toward enhanced separation and antibacterial performance, *J. Colloid Interface Sci.*, 2020, **572**, 114–121.

29 L. Cot, *et al.*, Inorganic membranes and solid state sciences, *Solid State Sci.*, 2000, **2**(3), 313–334.
30 T. A. Otitoju, A. L. Ahmad and B. S. Ooi, Recent advances in hydrophilic modification and performance of polyethersulfone (PES) membrane *via* additive blending, *RSC Adv.*, 2018, **8**(40), 22710–22728.
31 D. Koseoglu-Imer and I. Koyuncu, *Fabrication and Application Areas of Mixed Matrix Flat-Sheet Membranes*, 2017, pp. 49–66.
32 M. A. Alaei Shahmirzadi, *et al.*, Tailoring PES nanofiltration membranes through systematic investigations of prominent design, fabrication and operational parameters, *RSC Adv.*, 2015, **5**(61), 49080–49097.
33 N. Arahman, *et al.*, Fabrication of polyethersulfone membranes using nanocarbon as additive, *Int. J. GEOMATE*, 2018, **15**, 51–57.
34 A. Teella, *et al.*, Effects of chemical sanitization using NaOH on the properties of polysulfone and polyethersulfone ultrafiltration membranes, *Biotechnol. Prog.*, 2015, **31**(1), 90–96.
35 S. Petrin and M. Miteva, Effect of solvent and thermal treatment on the structure of polyacrylonitrile membranes, *Int. J. Sci. Res.*, 2012, **3**, 145–147.
36 Z. Fan, *et al.*, Preparation and characterization of polyaniline/polysulfone nanocomposite ultrafiltration membrane, *J. Membr. Sci.*, 2008, **310**(1), 402–408.
37 Z. Fan, *et al.*, Performance improvement of polysulfone ultrafiltration membrane by blending with polyaniline nanofibers, *J. Membr. Sci.*, 2008, **320**(1), 363–371.
38 S. De, *et al.*, Nanostructured polyaniline incorporated ultrafiltration membrane for desalination of brackish water, *Environ. Sci.: Water Res. Technol.*, 2015, **1**, 893–904.
39 A. Taghizadeh, *et al.*, Conductive polymers in water treatment: a review, *J. Mol. Liq.*, 2020, **312**, 113447.
40 P. Formoso, *et al.*, Electro-conductive membranes for permeation enhancement and fouling mitigation: a short review, *Membranes*, 2017, **7**(3), 39.
41 Khurram, *et al.*, Development of polyaniline based anion exchange membrane for the separation of lactic acid *via* electrodialysis, *Russ. J. Electrochem.*, 2020, **56**, 587–595.
42 H. Lin, C. Du and Z. Lin, Synthesis, Structure and Properties of Bacterial Cellulose/polyaniline/manganese Dioxide Nanocomposites *via* Layer-by-layer Interfacial Polymerization, *Mater. Sci. Res.*, 2014, **3**(1), 1.
43 A. Qaiser, M. Hyland and D. Patterson, Control of polyaniline deposition on microporous cellulose ester membranes by *in situ* chemical polymerization, *J. Phys. Chem. B*, 2009, **113**, 14986–14993.
44 M. Malik, A. Qaiser and M. Arif, Structural and electrochemical studies of heterogeneous ion exchange membranes based on polyaniline-coated cation exchange resin particles, *RSC Adv.*, 2016, **6**, 115046–115054.
45 M. Ahmad, *et al.*, Heterogeneous ion exchange membranes based on thermoplastic polyurethane (TPU): effect of PSS/DVB resin on morphology and electrodialysis, *RSC Adv.*, 2020, **10**, 3029–3039.
46 I. C. Kim, H.-G. Yun and K.-H. Lee, Preparation of asymmetric polyacrylonitrile membrane with small pore size by phase inversion and post-treatment process, *J. Membr. Sci.*, 2002, **199**, 75–84.
47 A. Saravanakumaar, *et al.*, Impact of alkali treatment on physico-chemical, thermal, structural and tensile properties of Carica papaya bark fibers, *Int. J. Polym. Anal. Charact.*, 2018, **23**(6), 529–536.
48 B. Malczewska and A. Żak, Structural Changes and Operational Deterioration of the Uf Polyethersulfone (Pes) Membrane Due to Chemical Cleaning, *Sci. Rep.*, 2019, **9**(1), 422.
49 M. K. Purkait and R. Singh, *Membrane Technology in Separation Science*, CRC Press, 2018.
50 A. Sotto, *et al.*, Doping of polyethersulfone nanofiltration membranes: antifouling effect observed at ultralow concentrations of TiO_2 nanoparticles, *J. Mater. Chem.*, 2011, **21**(28), 10311–10320.
51 C. Liao, *et al.*, Synthesis and characterization of low content of different SiO_2 materials composite poly (vinylidene fluoride) ultrafiltration membranes, *Desalination*, 2012, **285**, 117–122.
52 R. Nasir, *et al.*, Effect of fixed carbon molecular sieve (CMS) loading and various di-ethanolamine (DEA) concentrations on the performance of a mixed matrix membrane for CO_2/CH_4 separation, *RSC Adv.*, 2015, **5**(75), 60814–60822.
53 M. Farnam, H. Mukhtar and A. M. Shariff, An investigation of blended polymeric membranes and their gas separation performance, *RSC Adv.*, 2016, **6**(104), 102671–102679.
54 N. Kamal, *et al.*, Polysulfone membranes embedded with halloysites nanotubes: preparation and properties, *Membranes*, 2020, **10**(1), 2.
55 H. Yu, *et al.*, Improving the antifouling property of polyethersulfone ultrafiltration membrane by incorporation of dextran grafted halloysite nanotubes, *Chem. Eng. J.*, 2014, **237**, 322–328.
56 F. F. Ghiggi, *et al.*, Preparation and characterization of polyethersulfone/*N*-phthaloyl-chitosan ultrafiltration membrane with antifouling property, *Eur. Polym. J.*, 2017, **92**, 61–70.
57 S. Belfer, *et al.*, Surface characterization by FTIR–ATR spectroscopy of polyethersulfone membranes-unmodified, modified and protein fouled, *J. Membr. Sci.*, 2000, **172**(1–2), 113–124.
58 A. Rahimpour, *et al.*, Coupling TiO_2 nanoparticles with UV irradiation for modification of polyethersulfone ultrafiltration membranes, *J. Membr. Sci.*, 2008, **313**(1–2), 158–169.
59 H. A. Mannan, H. Mukhtar, and T. Murugesan, Preparation and characterization of newly developed polysulfone/polyethersulfone blend membrane for CO_2 separation, *Applied Mechanics and Materials*, Trans Tech Publ, 2015.
60 C.-H. Weng, Y.-T. Lin and T.-W. Tzeng, Removal of methylene blue from aqueous solution by adsorption onto pineapple leaf powder, *J. Hazard. Mater.*, 2009, **170**(1), 417–424.

61 K. Ajeel and Q. Kareem, Synthesis and characteristics of polyaniline (PANI) filled by graphene (PANI/GR) nano-films, *Journal of Physics: Conference Series*, IOP Publishing, 2019.

62 S. A. Kanhegaokar, *et al.*, Preparation of compatible polyaniline/polyethersulfone solution blends, *Polym. Bull.*, 2012, **69**(1), 95–104.

63 M. Farnam, H. Mukhtar and A. Shariff, Analysis of the influence of CMS variable percentages on pure PES membrane gas separation performance, *Procedia Eng.*, 2016, **148**, 1206–1212.

64 L. Wen, *et al.*, Decomposition kinetics of hydrogen bonds in coal by a new method of in-situ diffuse reflectance FT-IR, *J. Fuel Chem. Technol.*, 2011, **39**(5), 321–327.

65 V. Saadattalab, A. Shakeri and H. Gholami, Effect of CNTs and nano ZnO on physical and mechanical properties of polyaniline composites applicable in energy devices, *Prog. Nat. Sci.: Mater. Int.*, 2016, **26**(6), 517–522.

66 J. Rubio, M. Souza and R. Smith, Overview of flotation as a wastewater treatment technique, *Miner. Eng.*, 2002, **15**(3), 139–155.

67 A. A. Qaiser, M. M. Hyland and D. A. Patterson, Control of polyaniline deposition on microporous cellulose ester membranes by *in situ* chemical polymerization, *J. Phys. Chem. B*, 2009, **113**(45), 14986–14993.

68 A. J. Blok, *et al.*, Surface initiated polydopamine grafted poly([2-(methacryoyloxy)ethyl]trimethylammonium chloride) coatings to produce reverse osmosis desalination membranes with anti-biofouling properties, *J. Membr. Sci.*, 2014, **468**, 216–223.

69 M. Abdulsalam Ebrahim, S. Karan and A. G. Livingston, On the influence of salt concentration on the transport properties of reverse osmosis membranes in high pressure and high recovery desalination, *J. Membr. Sci.*, 2020, **594**, 117339.

70 I. Sapurina, A. Riede and J. Stejskal, *In situ* polymerized polyaniline films: 3. Film formation, *Synth. Met.*, 2001, **123**(3), 503–507.

71 J. Alam, *et al.*, Dye Separation and Antibacterial Activities of Polyaniline Thin Film-Coated Poly(phenyl sulfone) Membranes, *Membranes*, 2021, **11**, 25.

72 W. Shi, *et al.*, Enabling Superior Sodium Capture for Efficient Water Desalination by a Tubular Polyaniline Decorated with Prussian Blue Nanocrystals, *Adv. Mater.*, 2020, **32**, 1907404.

73 Y. Guo, *et al.*, High performance nanofiltration membrane using self-doping sulfonated polyaniline, *J. Membr. Sci.*, 2022, **652**, 120441.

74 J. Schaep, *et al.*, Retention Mechanisms in Nanofiltration, *Chemistry for the Protection of the Environment 3*, L. Pawłowski, et al., ed., Springer US, Boston, MA, 1998, pp. 117–125.

75 V. Geraldes, V. Semião and M. Pinho, Flow and Mass Transfer Modelling of Nanofiltration, *J. Membr. Sci.*, 2001, **191**, 109–128.

76 A. F. Ismail and T. Matsuura, *Membrane Separation Processes: Theories, Problems, and Solutions*, Elsevier Science, 2021.

77 J. Stejskal and R. G. Gilbert, Polyaniline. Preparation of a conducting polymer (IUPAC Technical Report), *Pure Appl. Chem.*, 2002, **74**(5), 857–867.

78 M. A. Shishov, V. A. Moshnikov and I. Y. Sapurina, Deposition of polyaniline layers with controlled thickness and morphology by *in situ* polymerization, *Russ. J. Appl. Chem.*, 2013, **86**(1), 51–62.

79 J. Yue and A. Epstein, XPS study of self-doped conducting polyaniline and parent systems, *Macromolecules*, 1991, **24**(15), 4441–4445.

80 Y. Zhang, Y. Duan and J. Liu, The Effect of Intermolecular Hydrogen Bonding on the Polyaniline Water Complex, *J. Cluster Sci.*, 2017, **28**(3), 1071–1081.

81 V. Vahid, Fabrication and characterization of novel antifouling nanofiltration membrane prepared from oxidized multiwalled carbon nanotube/polyethersulfone nanocomposite, *J. Membr. Sci.*, 2011, **375**(1–2), 284–294.

82 V. Vatanpour, M. Esmaeili and M. H. D. A. Farahani, Fouling reduction and retention increment of polyethersulfone nanofiltration membranes embedded by amine-functionalized multi-walled carbon nanotubes, *J. Membr. Sci.*, 2014, **466**, 70–81.

83 A. Somrani, A. H. Hamzaoui and M. Pontie, Study on lithium separation from salt lake brines by nanofiltration (NF) and low pressure reverse osmosis (LPRO), *Desalination*, 2013, **317**, 184–192.

84 M. Telzhensky, *et al.*, Selective separation of seawater Mg^{2+} ions for use in downstream water treatment processes, *Chem. Eng. J.*, 2011, **175**, 136–143.

85 M. Batool, *et al.*, TiO_2 Nanoparticle Filler-Based Mixed-Matrix PES/CA Nanofiltration Membranes for Enhanced Desalination, *Membranes*, 2021, **11**, 443–460.

86 Z. Wang, *et al.*, Nanoparticle-template nanofiltration membranes for ultrahigh performance desalination, *Nat. Commun.*, 2018, **9**, 2004–2014.

87 S. Zhu, *et al.*, Improved performance of polyamide thin-film composite nanofiltration membrane by using polyetersulfone/polyaniline membrane as the substrate, *J. Membr. Sci.*, 2015, **493**, 263–274.